Properties of MUSIC-Type Algorithm for Imaging of Thin Dielectric Inhomogeneity in Limited-View Inverse Scattering Problem

Won-Kwang Park*

Abstract—It is well known that a Multiple Signal Classification (MUSIC)-type algorithm yields good results in the imaging of thin dielectric inhomogeneity for full-view inverse scattering problems. In contrast, it yields a poor result in limited-view inverse scattering problems. In this paper, we verify the reason for the above by establishing a relationship between a MUSIC-type imaging function and the Bessel functions of the integer order of the first kind. This verification is based on the asymptotic expansion formula for thin dielectric inhomogeneity. Various numerical examples are discussed for confirming our verification.

1. INTRODUCTION

The main purpose of inverse scattering problems is to identify the unknown characteristics of unknown scatterers, such as locations, shapes, dielectric permittivities, and magnetic permeabilities. Most inverse scattering problems focus on shape reconstruction. Accordingly, various algorithms for shape reconstruction have been developed in the recent past. Most of these algorithms are based on Newton-type iteration schemes. Related works can be found in [1, 9, 22] and the references therein. However, for a successful application, an initial guess that is sufficiently close to the unknown target is required. If not, one must consider the significant amount of computational costs, local minimal problems, and non-convergence issues.

Alternatively, various non-iterative shape reconstruction methods have been investigated. Among them, the MUltiple SIgnal Classification (MUSIC) algorithm has been successfully applied to various problems such as the location search of small defects [3], anti-personnel mines [4], internal corrosion [5], and the shape identification of thin electromagnetic inhomogeneities and perfectly conducting cracks [6, 17, 19, 21]. However, in most of the studies that we mentioned above, the MUSIC algorithm has been applied only in full-view inverse scattering problems. In a limited-view problem such as the detection of inhomogeneities buried in a half-space problem considered in [4, 17], MUSIC produces very poor results. However, this fact has been observed only in the results via numerical simulation. Therefore, the development of a mathematical theory about the structure of the MUSIC algorithm is considered.

Recently, the structure of a MUSIC-type imaging function in a full-view problem has been established in [10]. However, the mathematical theory about its structure in a limited-view problem has not been established; it has, however, been used heuristically in many works. Motivated by this fact, we extend the recent work on structure analysis of MUSIC-type imaging in a full-view problem to the limited-view problem for the imaging of thin dielectric inhomogeneity by establishing a relationship between the MUSIC-type imaging function and the Bessel functions of integer order of the first kind. This is based on the fact that a measured far-field pattern can be written by an asymptotic expansion formula for the existence of thin inhomogeneity. From the derived structure, we can find out why the

* Corresponding author: Won-Kwang Park (parkwk@kookmin.ac.kr).
The author is with the Department of Mathematics, Kookmin University, Seoul 136-702, Korea.

MUSIC algorithm produces poor results in the limited-view problems and derive a condition for an acceptable imaging performance.

The remainder of this paper is organized as follows. In Section 2, we introduce two-dimensional direct scattering problems and the asymptotic expansion formula of a far-field pattern in the presence of thin dielectric inhomogeneity. In Section 2.1, we briefly mention the MUSIC-type imaging algorithm. Its structure and certain properties in the limited-view problem are respectively derived and discussed in Section 3. In Section 4, some numerical experiments are discussed for supporting the identified structure. A short conclusion is presented in Section 5.

2. DIRECT SCATTERING PROBLEMS AND FAR-FIELD PATTERN

In a two-dimensional homogeneous space $\mathbb{R}^2$, there exists thin, curve-like dielectric inhomogeneity Γ, which is localized in the neighborhood of a smooth curve σ such that

$$\Gamma = \{\mathbf{x} + \eta\mathbf{n}(\mathbf{x}) : \mathbf{x} \in \sigma, \ -h \leq \eta \leq h\},$$

where $\mathbf{n}(\mathbf{x})$ denotes the unit normal to σ at $\mathbf{x}$, and h denotes the thickness of Γ (see Figure 1). In this paper, we assume that $h \ll \lambda$, where λ denotes the given wavelength. Assume that every material is fully characterized by its dielectric permittivity at a given frequency $\omega = 2\pi/\lambda$. Let ε_0 and ε denote the permittivities of $\mathbb{R}^2$ and Γ, respectively. Throughout this paper, we assume that the magnetic permeabilities of Γ and $\mathbb{R}^2$ are same as μ_0.
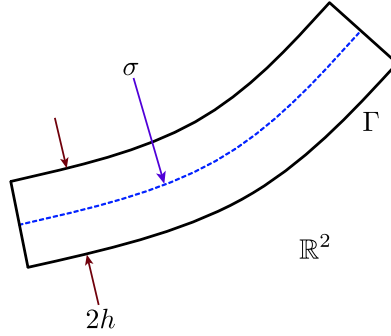

Figure 1. Two-dimensional thin dielectric inhomogeneity Γ with supporting curve σ.

For a given frequency, let $u(\mathbf{x})$ be the time-harmonic total field that satisfies the Helmholtz equation in the existence of Γ:

$$\frac{1}{\mu_0}\triangle u(\mathbf{x}) + \omega^2 \left(\varepsilon\chi(\Gamma) + \varepsilon_0\chi\left(\mathbb{R}^2\backslash\overline{\Gamma}\right)\right) u(\mathbf{x}) = 0 \quad \text{in} \quad \mathbb{R}^2. \tag{1}$$

Let $u_0(\mathbf{x}) = \exp(i\omega\boldsymbol{\theta} \cdot \mathbf{x})$ be the background solution and $u_s(\mathbf{x})$ be the unknown scattered field. Here, $\boldsymbol{\theta} = [\cos\theta, \sin\theta]^T$ represents a two-dimensional vector on the unit circle, $\mathbb{S}^1$ describes the direction, and $u_s(\mathbf{x})$ satisfies the Sommerfeld radiation condition

$$\lim_{|\mathbf{x}|\to\infty} \sqrt{|\mathbf{x}|} \left(\frac{\partial u_s(\mathbf{x})}{\partial |\mathbf{x}|} - ik_0u_s(\mathbf{x})\right) = 0$$

uniformly in all the directions $\hat{\mathbf{x}} = \mathbf{x}/|\mathbf{x}|$. Here, k_0 denotes the wavenumber $k_0 = \omega\sqrt{\varepsilon_0\mu_0}$. For the sake of simplicity, we set $\varepsilon_0 = 1$ and $\mu_0 = 1$, i.e., $k_0 = \omega$. The far-field pattern is defined as a function $u_\infty(\hat{\mathbf{y}}, \boldsymbol{\theta})$ that satisfies

$$u_s(\mathbf{y}) = \frac{\exp(i\omega|\mathbf{y}|)}{\sqrt{|\mathbf{y}|}} u_\infty(\hat{\mathbf{y}}, \boldsymbol{\theta}) + o\left(\frac{1}{\sqrt{|\mathbf{y}|}}\right)$$

as $|\mathbf{y}| \longrightarrow \infty$ uniformly on $\hat{\mathbf{y}} = \mathbf{y}/|\mathbf{y}|$ and $\boldsymbol{\theta} \in \mathbb{S}^1$. Then, the asymptotic formula for the far-field pattern can be represented as follows: Based on [7], it can be represented as follows:

Lemma 2.1. *[Asymptotic expansion formula] Let $u(\mathbf{x})$ satisfy (1); then, $u_\infty(\hat{\mathbf{y}}, \boldsymbol{\theta})$ can be represented as the following asymptotic expansion formula:*

$$u_\infty(\hat{\mathbf{y}}, \boldsymbol{\theta}) = h\frac{\omega^2(1+i)}{4\sqrt{\omega\pi}}\int_\sigma (\varepsilon - \varepsilon_0)\exp(i\omega(\boldsymbol{\theta} - \hat{\mathbf{y}})\cdot\mathbf{x})d\sigma(\mathbf{x}) + o(h), \tag{2}$$

where $o(h)$ is uniform in $\mathbf{x} \in \sigma$, $\hat{\mathbf{y}}, \boldsymbol{\theta} \in \mathbb{S}^1$.

2.1. Introduction to MUSIC Algorithm

In this section, we apply the asymptotic expansion formula (2) to introduce MUSIC algorithm. Before starting, we assume that for a given frequency ω, the thin inhomogeneity is divided into M different segments of the size of order $\lambda/2$. Considering the Rayleigh resolution limit from the far-field data, any detail less than one-half of the wavelength cannot be imaged, and only one point, say $\mathbf{x}_m$, $m = 1, 2, \ldots, M$, at each segment is imaged [3, 19, 21]. In this section, we denote a discrete finite set of the incident directions as $\{\boldsymbol{\theta}_1, \boldsymbol{\theta}_2, \ldots, \boldsymbol{\theta}_N\}$ and the same number of observation directions as $\{\boldsymbol{\vartheta}_1, \boldsymbol{\vartheta}_2, \ldots, \boldsymbol{\vartheta}_N\}$. The MUSIC algorithm is based on the structure of singular vectors linked to the non-zero singular vectors of the so-called Multi-Static Response (MSR) matrix $\mathbb{K}(\omega) = [K_{jl}(\omega)]_{j,l=1}^N$, whose element $K_{jl}(\omega) = u_\infty(\boldsymbol{\vartheta}_j, \boldsymbol{\theta}_l)$ is the far-field pattern collected at observation number j for the incident wave numbered l.

Let us consider the Singular Value Decomposition (SVD) on $\mathbb{K}$:

$$\mathbb{K}(\omega) = \mathbb{U}(\omega)\mathbb{S}(\omega)\mathbb{V}(\omega)^* = \sum_{m=1}^N \tau_m(\omega)\mathbf{U}_m(\omega)\mathbf{V}_m(\omega)^* \approx \sum_{m=1}^M \tau_m(\omega)\mathbf{U}_m(\omega)\mathbf{V}_m(\omega)^*,$$

where the superscript $*$ denotes the Hermitian matrix, $\mathbf{U}_m$ and $\mathbf{V}_m$ represent the left and right singular vectors of $\mathbb{K}$, and τ_m denotes the non-zero singular values that satisfy

$$\tau_1 \geq \tau_2 \geq \ldots \geq \tau_M \quad \text{and} \quad \tau_m \approx 0 \quad \text{for} \quad m = M+1, M+2, \ldots, N.$$

Then, since $\{\mathbf{U}_1, \mathbf{U}_2, \ldots, \mathbf{U}_M\}$ is the basis for the signal space of $\mathbb{K}$, we can define a projection operator onto the noise subspace:

$$\mathbf{P}_{\text{noise}} = \mathbb{I}(N) - \sum_{m=1}^M \mathbf{U}_m\mathbf{U}_m^*,$$

where $\mathbb{I}(N)$ denotes the $N \times N$ identity matrix. For any $\mathbf{z} \in \mathbb{R}^2$, define a test vector $\mathbf{f}(\mathbf{z})$ as

$$\mathbf{f}(\mathbf{z}) = \frac{1}{\sqrt{N}}[\exp(i\omega\boldsymbol{\theta}_1\cdot\mathbf{z}), \exp(i\omega\boldsymbol{\theta}_2\cdot\mathbf{z}), \ldots, \exp(i\omega\boldsymbol{\theta}_N\cdot\mathbf{z})]^T \tag{3}$$

and MUSIC-type imaging function

$$\mathcal{I}_{\text{MUSIC}}(\mathbf{z}; \omega) = \frac{1}{|\mathbf{P}_{\text{noise}}(\mathbf{f}(\mathbf{z}); \omega)|}.$$

Then, $\mathcal{I}_{\text{MUSIC}}(\mathbf{z}; \omega)$ will plot the peaks of a large magnitude at $\mathbf{z} \in \sigma$ and those of a small magnitude at $\mathbf{z} \notin \Gamma$.

3. STRUCTURE OF MUSIC-TYPE IMAGING FUNCTION IN LIMITED-VIEW PROBLEM

We explore the structure of a MUSIC-type imaging function in the limited-view inverse scattering problems. For this, we assume that $0 < \theta_1 < \theta_2 < \ldots < \theta_N < 2\pi$ and $\boldsymbol{\theta}_n \in \mathbb{S}^1_* \subsetneq \mathbb{S}^1$ for $n = 1, 2, \ldots, N$. For the sake of simplicity, we exclude the constant $h\omega^2(1+i)/(4\sqrt{\omega\pi})$ and the residue term $o(h)$ in (2) and assume that the incident and observation directions are the same, i.e., $\boldsymbol{\vartheta}_j = -\boldsymbol{\theta}_j$ for $j = 1, 2, \ldots, N$. Then,

$$K_{jl}(\omega) \approx \int_\sigma (\varepsilon - 1)\exp(i\omega(\boldsymbol{\theta}_j + \boldsymbol{\theta}_l)\cdot\mathbf{x})d\sigma(\mathbf{x}) \approx \frac{\text{length}(\sigma)}{M}\sum_{m=1}^M (\varepsilon - 1)\exp(i\omega(\boldsymbol{\theta}_j + \boldsymbol{\theta}_l)\cdot\mathbf{x}_m), \tag{4}$$

where length(σ) denotes the length of σ (refer to [21]). Based on this, $\mathbb{K}$ can be decomposed as follows:

$$\mathbb{K} = \frac{\text{length}(\sigma)}{M}(\varepsilon - 1) \sum_{m=1}^{M} \mathbf{W}(\mathbf{x}_m)\mathbf{W}(\mathbf{x}_m)^T,$$

where $\mathbf{W}(\mathbf{y})$ is defined in (5). Then, the following result holds.

Lemma 3.1. *For $\boldsymbol{\theta}_n \in \mathbb{S}_*^1$, define*

$$\mathbf{W}(\mathbf{z}) = \frac{1}{\sqrt{N}} \left[\exp(i\omega\boldsymbol{\theta}_1 \cdot \mathbf{z}), \exp(i\omega\boldsymbol{\theta}_2 \cdot \mathbf{z}), \ldots, \exp(i\omega\boldsymbol{\theta}_N \cdot \mathbf{z})\right]^T. \tag{5}$$

Then, $\mathbf{U}_m \approx \mathbf{W}(\mathbf{x}_m)$ for $m = 1, 2, \ldots, M$.

Further, we introduce a useful formula that describes a relationship between a definite integration of the exponential function on the subset of a unit circle and the Bessel function of an integer order of the first kind. A rigorous derivation can be found in [11].

Lemma 3.2. *For $\boldsymbol{\theta} \in \mathbb{S}_*^1$ and $\mathbf{z} = |\mathbf{z}|[\cos\phi, \sin\phi]^T \in \mathbb{R}^2$, the following approximation holds uniformly*

$$\frac{1}{N} \sum_{n=1}^{N} \exp(i\omega\boldsymbol{\theta}_n \cdot \mathbf{z}) \approx \frac{1}{\theta_N - \theta_1} \int_{\mathbb{S}_*^1} \exp(i\omega\boldsymbol{\theta} \cdot \mathbf{z})d\boldsymbol{\theta} = J_0(\omega|\mathbf{z}|) + \frac{\Xi(\mathbf{z};\omega)}{\theta_N - \theta_1},$$

where J_n denotes the Bessel function of order n of the first kind and $\Xi(\mathbf{z};\omega)$ is given by

$$\Xi(\mathbf{z};\omega) = 4\sum_{n=1}^{\infty} \frac{i^n}{n} J_n(\omega|\mathbf{z}|) \sin\left(\frac{n(\theta_N - \theta_1)}{2}\right) \cos\left(\frac{n(\theta_N + \theta_1 - 2\phi)}{2}\right).$$

Now, we derive the structure of single-frequency MUSIC-type imaging function in the limited-view problem.

Theorem 3.3 (Single-frequency MUSIC). *Let ω and N be sufficiently large. Let us write $\mathbf{z} - \mathbf{x}_m = |\mathbf{z} - \mathbf{x}_m|[\cos\phi_m, \sin\phi_m]^T$ then, $\mathcal{I}_{\text{MUSIC}}(\mathbf{z};\omega)$ is of the form:*

$$\mathcal{I}_{\text{MUSIC}}(\mathbf{z};\omega) = \left\{1 - \sum_{m=1}^{M} \left|J_0(\omega|\mathbf{z} - \mathbf{x}_m|) + \frac{\Xi(\mathbf{z} - \mathbf{x}_m;\omega)}{\theta_N - \theta_1}\right|^2\right\}^{-1/2}, \tag{6}$$

where $|c|^2 = c\bar{c}$ for a complex number c.

Proof. Let us apply Lemma 3.1 to the projection operator. Then,

$$\mathbf{P}_{\text{noise}}(\mathbf{f}(\mathbf{z});\omega) \approx \left(\mathbb{I} - \frac{1}{N}\sum_{m=1}^{M} \mathbf{W}(\mathbf{x}_m)\mathbf{W}(\mathbf{x}_m)^*\right)\mathbf{f}(\mathbf{z}) = \frac{1}{\sqrt{N}}\begin{bmatrix} \exp(i\omega\boldsymbol{\theta}_1 \cdot \mathbf{z}) \\ \exp(i\omega\boldsymbol{\theta}_2 \cdot \mathbf{z}) \\ \vdots \\ \exp(i\omega\boldsymbol{\theta}_N \cdot \mathbf{z}) \end{bmatrix} - \frac{1}{N\sqrt{N}}\sum_{m=1}^{M} \mathbb{A},$$

where

$$\mathbb{A} = \begin{bmatrix} \exp(i\omega\boldsymbol{\theta}_1 \cdot \mathbf{z}) + \sum\limits_{n\in\mathbb{N}_1} \exp\{i\omega(\boldsymbol{\theta}_1 \cdot \mathbf{x}_m + \boldsymbol{\theta}_n \cdot (\mathbf{z} - \mathbf{x}_m))\} \\ \exp(i\omega\boldsymbol{\theta}_2 \cdot \mathbf{z}) + \sum\limits_{n\in\mathbb{N}_2} \exp\{i\omega(\boldsymbol{\theta}_2 \cdot \mathbf{x}_m + \boldsymbol{\theta}_n \cdot (\mathbf{z} - \mathbf{x}_m))\} \\ \vdots \\ \exp(i\omega\boldsymbol{\theta}_N \cdot \mathbf{z}) + \sum\limits_{n\in\mathbb{N}_N} \exp\{i\omega(\boldsymbol{\theta}_N \cdot \mathbf{x}_m + \boldsymbol{\theta}_n \cdot (\mathbf{z} - \mathbf{x}_m))\} \end{bmatrix}$$

Here, $\mathbb{N}_s := \{1, 2, \ldots, N\}\setminus\{s\}$. Since,

$$\exp(i\omega\boldsymbol{\theta}_s \cdot \mathbf{z}) = \exp(i\omega\boldsymbol{\theta}_s \cdot \mathbf{x}_m)\exp\{i\omega\boldsymbol{\theta}_s \cdot (\mathbf{z} - \mathbf{x}_m)\},$$

plugging this into $\mathbb{A}$ and applying Lemma 3.2, we can obtain

$$\frac{1}{N} \sum_{m=1}^{M} \left(\exp(i\omega\boldsymbol{\theta}_s \cdot \mathbf{z}) + \sum_{n\in\mathbb{N}_s} \exp\{i\omega(\boldsymbol{\theta}_s \cdot \mathbf{x}_m + \boldsymbol{\theta}_n \cdot (\mathbf{z} - \mathbf{x}_m))\} \right)$$

$$= \sum_{m=1}^{M} \exp(i\omega\boldsymbol{\theta}_s \cdot \mathbf{x}_m) \left(\frac{1}{N} \sum_{n=1}^{N} \exp\{i\omega\boldsymbol{\theta}_n \cdot (\mathbf{z} - \mathbf{x}_m)\} \right)$$

$$= \sum_{m=1}^{M} \exp(i\omega\boldsymbol{\theta}_s \cdot \mathbf{x}_m) \left(J_0(\omega|\mathbf{z} - \mathbf{x}_m|) + \frac{\Xi(\mathbf{z} - \mathbf{x}_m; \omega)}{\theta_N - \theta_1} \right).$$

Hence, $\mathbf{P}_{\text{noise}}(\mathbf{f}(\mathbf{z}); \omega)$ becomes

$$\mathbf{P}_{\text{noise}}(\mathbf{f}(\mathbf{z}); \omega) = \frac{1}{\sqrt{N}} \begin{bmatrix} \exp(i\omega\boldsymbol{\theta}_1 \cdot \mathbf{z}) - \sum_{m=1}^{M} \Lambda_m \exp(i\omega\boldsymbol{\theta}_1 \cdot \mathbf{x}_m) \\ \exp(i\omega\boldsymbol{\theta}_2 \cdot \mathbf{z}) - \sum_{m=1}^{M} \Lambda_m \exp(i\omega\boldsymbol{\theta}_2 \cdot \mathbf{x}_m) \\ \vdots \\ \exp(i\omega\boldsymbol{\theta}_N \cdot \mathbf{z}) - \sum_{m=1}^{M} \Lambda_m \exp(i\omega\boldsymbol{\theta}_N \cdot \mathbf{x}_m) \end{bmatrix},$$

where

$$\Lambda_m := J_0(\omega|\mathbf{z} - \mathbf{x}_m|) + \frac{\Xi(\mathbf{z} - \mathbf{x}_m; \omega)}{\theta_N - \theta_1}.$$

Therefore, we can obtain

$$|\mathbf{P}_{\text{noise}}(\mathbf{f}(\mathbf{z}); \omega)| = \left(\mathbf{P}_{\text{noise}}(\mathbf{f}(\mathbf{z}); \omega) \cdot \overline{\mathbf{P}_{\text{noise}}(\mathbf{f}(\mathbf{z}); \omega)} \right)^{1/2} = \left(\frac{1}{N} \sum_{n=1}^{N} \left\{ 1 - 2\mathrm{Re}(f_1) + f_2\overline{f}_2 \right\} \right)^{1/2},$$

where

$$f_1 := \sum_{m=1}^{M} \overline{\Lambda}_m \exp(i\omega\boldsymbol{\theta}_n \cdot (\mathbf{z} - \mathbf{x}_m)) \quad \text{and} \quad f_2 := \sum_{m=1}^{M} \Lambda_m \exp(i\omega\boldsymbol{\theta}_n \cdot \mathbf{x}_m).$$

Now, applying Lemma 3.2 again, we can obtain

$$\frac{1}{N} \sum_{n=1}^{N} f_1 = \frac{1}{N} \sum_{n=1}^{N} \sum_{m=1}^{M} \overline{\Lambda}_m \exp\{i\omega\boldsymbol{\theta}_n \cdot (\mathbf{z} - \mathbf{x}_m)\}$$

$$= \sum_{m=1}^{M} \overline{\Lambda}_m \left(\frac{1}{N} \sum_{n=1}^{N} \exp\{i\omega\boldsymbol{\theta}_n \cdot (\mathbf{z} - \mathbf{x}_m)\} \right) = \sum_{m=1}^{M} |\Lambda_m|^2. \tag{7}$$

Since ω is sufficiently large, following asymptotic form of Bessel function holds

$$J_n(\omega x) = \sqrt{\frac{2}{\omega x \pi}} \cos\left(\omega x - \frac{n\pi}{2} - \frac{\pi}{4} + O\left(\frac{1}{|\omega x|} \right) \right). \tag{8}$$

Hence, if $m \neq m'$,

$$J_0(\omega|\mathbf{x}_m - \mathbf{x}_{m'}|) + \frac{\Xi(\mathbf{x}_m - \mathbf{x}_{m'})}{\theta_N - \theta_1} \longrightarrow 0.$$

Therefore, by using Lemma 3.2, we can evaluate the following:

$$\frac{1}{N}\sum_{n=1}^{N} f_2\overline{f}_2 = \frac{1}{N}\sum_{n=1}^{N}\sum_{m=1}^{M}\sum_{m'=1}^{M}\Lambda_m\overline{\Lambda}_{m'}\exp\{i\omega\boldsymbol{\theta}_n\cdot(\mathbf{x}_m-\mathbf{x}_{m'})\}$$

$$= \sum_{m=1}^{M}\sum_{m'=1}^{M}\Lambda_m\overline{\Lambda}_{m'}\left(\frac{1}{N}\sum_{n=1}^{N}\exp\{i\omega\boldsymbol{\theta}_n\cdot(\mathbf{x}_m-\mathbf{x}_{m'})\}\right) = \sum_{m=1}^{M}\Lambda_m\overline{\Lambda}_m = \sum_{m=1}^{M}|\Lambda_m|^2. \quad (9)$$

Therefore, by using (7) and (9), we can obtain (6). This completes the proof.   □

Based on recent works [3, 10, 11, 15, 20], multi-frequency based imaging function yields better results than single-frequency based one. In contrast, in the limited-view problem, one cannot obtain a good result via multi-frequency MUSIC algorithm, refer to [16]. However, this fact has been identified heuristically so that mathematical identification is still required. Motivated from this fact, we now explore the structure of the multi-frequency MUSIC-type imaging to identify this phenomenon. For given S-different frequencies $\{\omega_s : s = 1, 2, \ldots, S\}$, let us introduce following multi-frequency MUSIC-type imaging function:

$$\mathcal{I}_{\text{MULTI}}(\mathbf{z}; S) := \left|\frac{1}{S}\sum_{s=1}^{S}\mathbf{P}_{\text{noise}}(\mathbf{f}(\mathbf{z}); \omega_s)\right|^{-1}.$$

Then, applying Theorem 3.3, we can immediately obtain following result.

Theorem 3.4 (Multi-frequency MUSIC). *Assume that ω_s, S, and N are sufficiently large. Let us write $\mathbf{z} - \mathbf{x}_m = |\mathbf{z} - \mathbf{x}_m|[\cos\phi_m, \sin\phi_m]^T$. Then, multi-frequency MUSIC-type imaging function can be represented as follows:*

$$\mathcal{I}_{\text{MULTI}}(\mathbf{z}; S) = \left\{1 - \sum_{m=1}^{M}\left|\Phi(\mathbf{z} - \mathbf{x}_m; \omega_1, \omega_S) + \frac{\Psi(\mathbf{z} - \mathbf{x}_m; \omega_1, \omega_S)}{\theta_N - \theta_1}\right|^2\right\}^{-1/2}, \quad (10)$$

where

$$\Phi(x; \omega_1, \omega_S) \approx \frac{\omega_S}{\omega_S - \omega_1}\left(J_0(\omega_S|x|)^2 + J_1(\omega_S|x|)^2\right) - \frac{\omega_1}{\omega_S - \omega_1}\left(J_0(\omega_1|x|)^2 + J_1(\omega_1|x|)^2\right) + \int_{\omega_1}^{\omega_S}J_1(\omega|x|)^2 d\omega$$

and

$$\Psi(\mathbf{z} - \mathbf{x}_m; \omega_1, \omega_S) \approx \int_{\omega_1}^{\omega_S}\Xi(\mathbf{z} - \mathbf{x}_m; \omega)d\omega$$

$$= 4\sum_{n=1}^{\infty}\frac{i^n}{n}\sin\left(\frac{n(\theta_N - \theta_1)}{2}\right)\cos\left(\frac{n(\theta_N + \theta_1 - 2\phi_m)}{2}\right)\int_{\omega_1}^{\omega_S}J_n(\omega|\mathbf{z} - \mathbf{x}_m|)d\omega.$$

Proof. Applying Theorem 3.3 and following an indefinite integral of the Bessel function (see [23])

$$\int J_0(x)^2 dx = x\left(J_0(x)^2 + J_1(x)^2\right) + \int J_1(x)^2 dx,$$

we can immediate obtain desired result.   □

Remark 3.5. *Theorems 3.3 and 3.4 tell us some properties that can be summarized as follows:*

(S1) *In the structure of MUSIC-type imaging function, the terms $J_0(\omega|\mathbf{z} - \mathbf{x}_m|)$ and $\Phi(\mathbf{z} - \mathbf{x}_m; \omega_1, \omega_S)$ contribute to the imaging performance. In contrast, the terms $\Xi(\mathbf{z}; \omega)$ and $\Psi(\mathbf{z} - \mathbf{x}_m; \omega_1, \omega_S)$ disturb the imaging performance.*

(S2) *On the basis of the asymptotic property of the Bessel function (8), a good result can be obtained via MUSIC algorithm when $\omega \longrightarrow +\infty$. However, this is an ideal condition.*

(S3) *Since $\Phi(\mathbf{z}-\mathbf{x}_m;\omega_1,\omega_S)$ oscillates less than $J_0(\omega|\mathbf{z}-\mathbf{x}_m|)$, it is expected that multi-frequency MUSIC improves single-frequency one. However, if the range of the incident (and observation) directions is narrow, then since $\theta_N - \theta_1$ is small,*

$$J_0(\omega|\mathbf{z}-\mathbf{x}_m|) \ll \frac{\Xi(\mathbf{z};\omega)}{\theta_N - \theta_1} \quad and \quad \Phi(\mathbf{z}-\mathbf{x}_m;\omega_1,\omega_S) \ll \frac{\Psi(\mathbf{z}-\mathbf{x}_m;\omega_1,\omega_S)}{\theta_N - \theta_1}.$$

Hence, the results via $\mathcal{I}_{\mathrm{MUSIC}}(\mathbf{z};\omega)$ and $\mathcal{I}_{\mathrm{MULTI}}(\mathbf{z};S)$ would be poor, i.e., there is no improvement. This is the reason why one cannot obtain good results via single- and multi-frequency MUSIC algorithms in limited-view problems. In contrast, if the range of the incident directions is sufficiently wide, one can obtain good results via MUSIC algorithm and $\mathcal{I}_{\mathrm{MULTI}}(\mathbf{z};S)$ will improve $\mathcal{I}_{\mathrm{MUSIC}}(\mathbf{z};\omega)$.

(S4) *On the basis of Lemma 3.2, if we can control the range of the incident directions such that*

$$\sin\left(\frac{n(\theta_N - \theta_1)}{2}\right) \cos\left(\frac{n(\theta_N + \theta_1 - 2\phi_m)}{2}\right) = 0$$

then, since the disturbing terms are disappear, one can obtain a good result. However, this is only the case $\theta_N - \theta_1 = 2\pi$, i.e., full-view inverse problem because we have no a priori information of thin inhomogeneities. Therefore, in the case of the limited-view inverse scattering problems, we cannot expect a good result via MUSIC algorithm.

4. NUMERICAL RESULTS AND DISCUSSION

In order to support Theorems 3.3 and 3.4, we present some numerical examples. For this, we consider the imaging of thin dielectric inhomogeneities $\Gamma_j = \{\mathbf{x} + \eta\mathbf{n}(\mathbf{x}) : \mathbf{x} \in \sigma_j, \; -h \leq \eta \leq h\}$ with two supporting curves

$$\sigma_1 = \left\{[s, 0.2]^T : -0.5 \leq s \leq 0.5\right\}$$

$$\sigma_2 = \left\{\left[s, \frac{1}{2}\cos\frac{s\pi}{2} + \frac{1}{5}\sin\frac{s\pi}{2} - \frac{1}{10}\cos\frac{3s\pi}{2}\right]^T : -1 \leq s \leq 1\right\}$$

with the same thickness $h = 0.02$. Permittivities of the background space and the thin inhomogeneity are selected as $\varepsilon_0 = 1$ and $\varepsilon = 5$, respectively, and permeability is $\mu_0 = 1$. Throughout this section, the
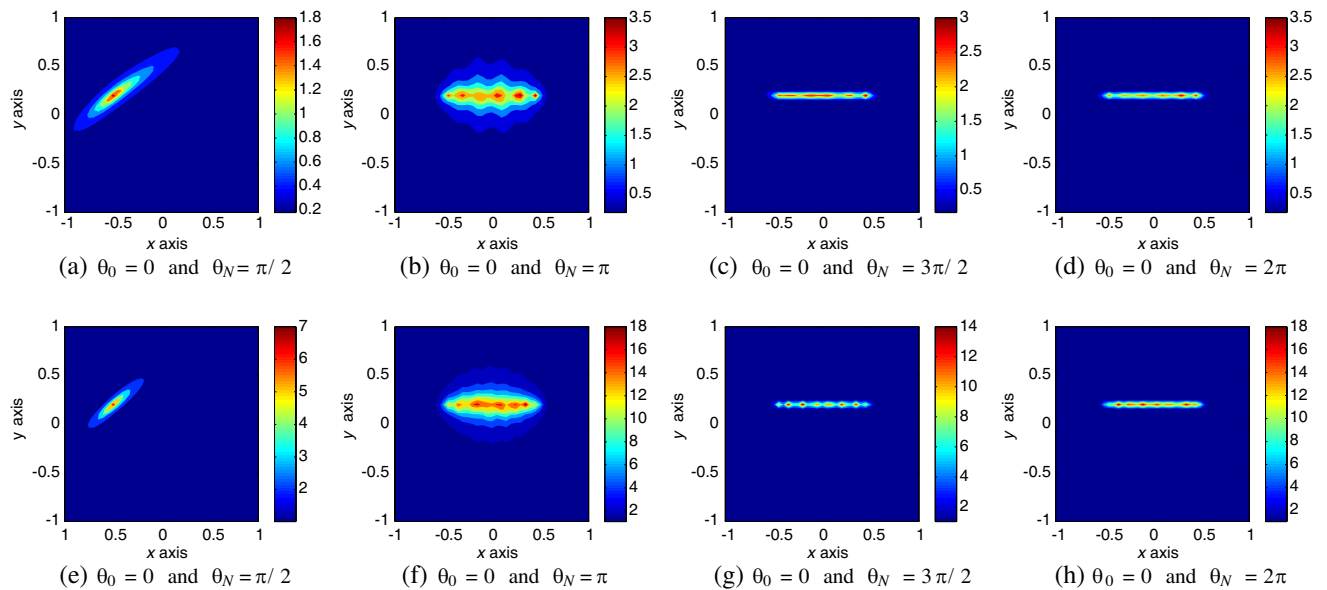

(a) $\theta_0 = 0$ and $\theta_N = \pi/2$ (b) $\theta_0 = 0$ and $\theta_N = \pi$ (c) $\theta_0 = 0$ and $\theta_N = 3\pi/2$ (d) $\theta_0 = 0$ and $\theta_N = 2\pi$

(e) $\theta_0 = 0$ and $\theta_N = \pi/2$ (f) $\theta_0 = 0$ and $\theta_N = \pi$ (g) $\theta_0 = 0$ and $\theta_N = 3\pi/2$ (h) $\theta_0 = 0$ and $\theta_N = 2\pi$

Figure 2. Maps of $\mathcal{I}_{\mathrm{MUSIC}}(\mathbf{z};\omega_1)$ (top) and $\mathcal{I}_{\mathrm{MULTI}}(\mathbf{z};10)$ (bottom) when the thin inhomogeneity is Γ_1.

wavelengthes λ_s, $s = 1, 2, \ldots, S(= 10)$, satisfy $\lambda_1 > \lambda_2 > \ldots > \lambda_S$ and

$$\lambda_1 = 0.5 \times \text{length}(\sigma_1) = 0.5 \quad \text{and} \quad \lambda_S = 0.2 \times \text{length}(\sigma_1) = 0.2.$$

In every results, the far-field pattern $u_\infty(\boldsymbol{\vartheta}_j, \boldsymbol{\theta}_l)$ computed by a second-kind integral equation introduced in [14].

Figure 2 shows the maps of $\mathcal{I}_{\text{MUSIC}}(\mathbf{z}; \omega_1)$ with various ranges of incident directions when the thin inhomogeneity is Γ_1. This result shows that when the range of incident directions is narrow (see Figure 2(a)), based on the observation (S3) of Remark 3.5, one cannot identify the true shape of Γ_1. In contrast, in Figure 2(b), although some blurring effect appeared in the neighborhood of Γ_1, we can recognize the approximate shape of Γ_1 when $\theta_0 = 0$ and $\theta_N = \pi$. Note that if $\theta_1 = 0$ and $\pi \leq \theta_N \leq 2\pi$, very good results appear.

Figure 3 shows the maps of $\mathcal{I}_{\text{MUSIC}}(\mathbf{z}; \omega_1)$ for Γ_2. In contrast to the results shown in Figure 2, the true shape of Γ_2 can be obtained in the full-view configuration. Hence, we conclude that if one wants to image a complex shaped target, the range of incident (and observation) directions must be sufficiently wide as we observed in (S4) of Remark 3.5.
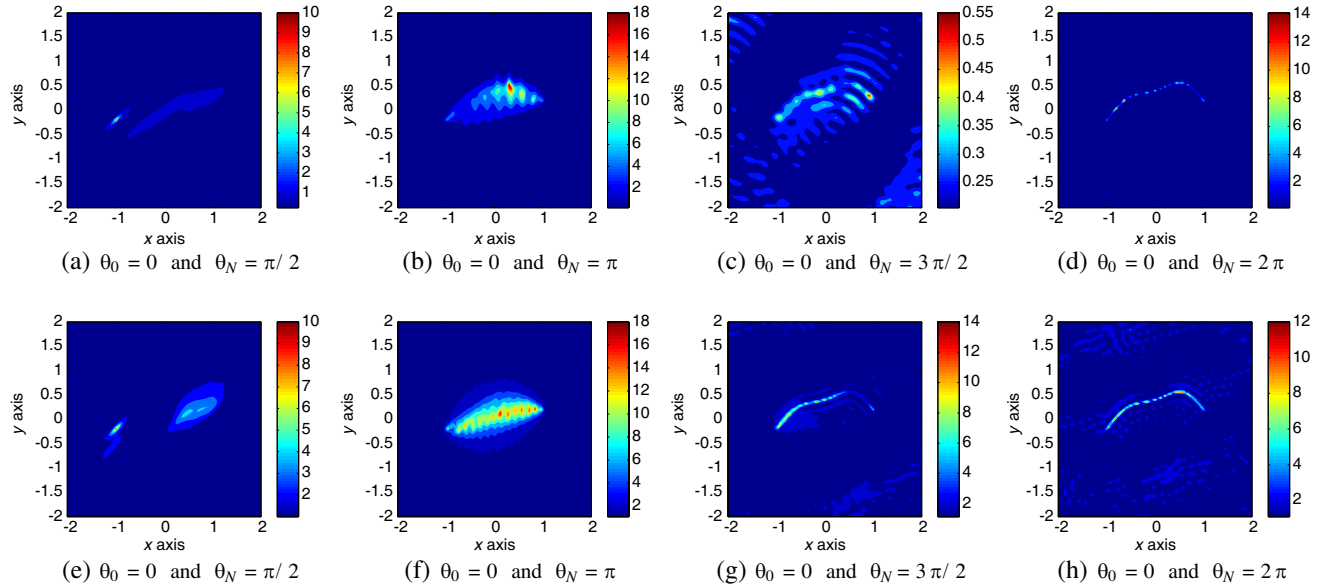

(a) $\theta_0 = 0$ and $\theta_N = \pi/2$ (b) $\theta_0 = 0$ and $\theta_N = \pi$ (c) $\theta_0 = 0$ and $\theta_N = 3\pi/2$ (d) $\theta_0 = 0$ and $\theta_N = 2\pi$

(e) $\theta_0 = 0$ and $\theta_N = \pi/2$ (f) $\theta_0 = 0$ and $\theta_N = \pi$ (g) $\theta_0 = 0$ and $\theta_N = 3\pi/2$ (h) $\theta_0 = 0$ and $\theta_N = 2\pi$

Figure 3. Same as Figure 2 except the thin inhomogeneity is Γ_2.

5. CONCLUSION

In this paper, we discovered the structure of the MUSIC-type imaging function of thin dielectric inhomogeneity located in the two-dimensional homogeneous space in the limited-view inverse scattering problems. On the basis of the relationship between the imaging function and the Bessel functions of the integer order of the first kind, we identified certain properties of the MUSIC algorithm in the limited-view inverse scattering problems.

In this paper, the imaging of thin dielectric inhomogeneity was considered. We believe that the analysis could be extended for a purely magnetic contrast between the inclusions and the embedding domain, and the combined cases. Furthermore, extension of the analysis to the imaging of a perfectly conducting, arbitrary shaped crack is expected.

Note that topological derivative based non-iterative imaging algorithm has been developed but considered only in full-aperture inverse scattering problems, refer to [2, 12, 13, 15, 17, 18]. Motivated from this fact, an analysis of topological derivative imaging function in the limited-aperture problem should be an interesting work.

ACKNOWLEDGMENT

REFERENCES

1. Álvarez, D., O. Dorn, N. Irishina, and M. Moscoso, "Crack reconstruction using a level-set strategy," *J. Comput. Phys.*, Vol. 228, 5710–5721, 2009.

2. Ammari H., J. Garnier, V. Jugnon, and H. Kang, "Stability and resolution analysis for a topological derivative based imaging functional," *SIAM J. Control. Optim.*, Vol. 50, 48–76, 2012.

3. Ammari H., J. Garnier, H. Kang, W.-K. Park, and K. Sølna, "Imaging schemes for perfectly conducting cracks," *SIAM J. Appl. Math.*, Vol. 71, 68–91, 2011.

4. Ammari, H., E. Iakovleva, and D. Lesselier, "A MUSIC algorithm for locating small inclusions buried in a half-space from the scattering amplitude at a fixed frequency," *SIAM Multiscale Modeling Simulation*, Vol. 3, 597–628, 2005.

5. Ammari, H., H. Kang, E. Kim, K. Louati, and M. S. Vogelius, "A MUSIC-type algorithm for detecting internal corrosion from electrostatic boundary measurements," *Numer. Math.*, Vol. 108, 501–528, 2008.

6. Ammari, H., H. Kang, H. Lee, and W.-K. Park, "Asymptotic imaging of perfectly conducting cracks," *SIAM J. Sci. Comput.*, Vol. 32, 894–922, 2010.

7. Beretta, E. and E. Francini, "Asymptotic formulas for perturbations of the electromagnetic fields in the presence of thin imperfections," *Contemp. Math.*, Vol. 333, 49–63, 2003.

8. Chen, X. and Y. Zhong, "MUSIC electromagnetic imaging with enhanced resolution for small inclusions," *Inverse Problems*, Vol. 25, 015008, 2009.

9. Dorn O. and D. Lesselier, "Level set methods for inverse scattering," *Inverse Problems*, Vol. 22, R67–R131, 2006.

10. Joh, Y.-D. and W.-K. Park, "Structural behavior of the MUSIC-type algorithm for imaging perfectly conducting cracks," *Progress In Electromagnetics Research*, Vol. 138, 211–226, 2013.

11. Kwon, Y. M. and W.-K. Park, "Analysis of subspace migration in the limited-view inverse scattering problems," *Appl. Math. Lett.*, Vol. 26, 1107–1113, 2013.

12. Ma, Y.-K., P.-S. Kim, and W.-K. Park, "Analysis of topological derivative function for a fast electromagnetic imaging of perfectly conducing cracks," *Progress In Electromagnetics Research*, Vol. 122, 311–325, 2012.

13. Ma, Y.-K. and W.-K. Park, "A topological derivative based non-iterative electromagnetic imaging of perfectly conducting cracks," *J. Electromagn. Eng. Sci.*, Vol. 12, 128–134, 2012.

14. Nazarchuk, Z. and K. Kobayashi, "Mathematical modelling of electromagnetic scattering from a thin penetrable target," *Progress In Electromagnetics Research*, Vol. 55, 95–116, 2005.

15. Park, W.-K., "Multi-frequency topological derivative for approximate shape acquisition of curve-like thin electromagnetic inhomogeneities," *J. Math. Anal. Appl.*, Vol. 402, 501–518, 2013.

16. Park W.-K., "On the imaging of thin dielectric inclusions buried within a half-space," *Inverse Problems*, Vol. 26, 074008, 2010.

17. Park, W.-K., "On the imaging of thin dielectric inclusions via topological derivative concept," *Progress In Electromagnetics Research*, Vol. 110, 237–252, 2010.

18. Park, W.-K., "Topological derivative strategy for one-step iteration imaging of arbitrary shaped thin, curve-like electromagnetic inclusions," *J. Comput. Phys.*, Vol. 231, 1426–1439, 2012.

19. Park, W.-K. and D. Lesselier, "Electromagnetic MUSIC-type imaging of perfectly conducting, arc-like cracks at single frequency," *J. Comput. Phys.*, Vol. 228, 8093–8111, 2009.

20. Park, W.-K. and D. Lesselier, "Fast electromagnetic imaging of thin inclusions in half-space affected by random scatterers," *Waves Random Complex Media*, Vol. 22, 3–23, 2012.

21. Park, W.-K. and D. Lesselier, "MUSIC-type imaging of a thin penetrable inclusion from its far-field multi-static response matrix," *Inverse Problems*, Vol. 25, 075002, 2009.

22. Park, W.-K. and D. Lesselier, "Reconstruction of thin electromagnetic inclusions by a level set method," *Inverse Problems*, Vol. 25, 085010, 2009.

23. Rosenheinrich, W., "Tables of some indefinite integrals of bessel functions," available at http://www.fh-jena.de/~rsh/Forschung/Stoer/besint.pdf.

24. Solimene, R., A. Dell'Aversano, and G. Leone, "Interferometric time reversal MUSIC for small scatterer localization," *Progress In Electromagnetics Research,* Vol. 131, 243–258, 2012.